Optical Materials 122 (2021) 111750

Contents lists available at ScienceDirect

Optical Materials

journal homepage: www.elsevier.com/locate/optmat

Spectroscopic study, theoretical calculations, and optical nonlinear properties of amino acid (glycine)-4-nitro benzaldeyhyde-derived Schiff base

Ahmed Majeed Jassem [a], Qusay M.A. Hassan [b,*], Faeza Abdulkareem Almashal [a], H.A. Sultan [b], Adil Muala Dhumad [a], C.A. Emshary [b], Luma Taher Tuma Albaaj [a]

[a] Department of Chemistry, College of Education for Pure Sciences, University of Basrah, Basrah, 61001, Iraq
[b] Department of Physics, College of Education for Pure Sciences, University of Basrah, Basrah, 61001, Iraq

ARTICLE INFO

Keywords:
Schiff base
RDPs
Z-scan
NIR
OLg

ABSTRACT

Schiff base of amino acid salt: potassium 2-((4-nitrobenzylidene)amino)acetate **4** ($C_9H_7KN_2O_4$), derived from the condensation reaction of amino acid (glycine) **1** and 4-nitro benzaldeyhyde **3** is synthesized and fully characterized by magnetic nuclear resonance (^1H and ^{13}C NMR), infrared (IR), mass, UV–visible spectroscopies and melting point. The optical nonlinear (ONL) properties of amino acid Schiff base salt 4 are studied using continuous wave (cw), visible, single transverse fundamental mode, low power, 473 nm laser beam. Ring diffraction patterns (RDPs) and Z-scan techniques are adopted to calculate the nonlinear index of refraction (NIR) together with testing the sample property of optical limiting (OLg). RDPs are simulated numerically using the integral of Fresnel-Kirchhoff and compared with experimental findings.

1. Introduction

Recently, interest has been growing in the investigation of optical nonlinear (ONL) properties of various organic materials. The study of the ONL properties are carried out using three different techniques viz., spatial self-phase modulation [1] (SSPM), thermal lens (TL) [2], and the open and closed apertures Z-scans [3]. The passage of a Gaussian continuous wave (cw), single fundamental, TEM_{00}, mode laser beam through a nonlinear medium, resulted in phenomena in the transverse dimensions viz., SSPM, self-focusing (SF) and self-defocusing (SDF), beam break-up, optical switching, optical bi stability, optical solitons, optical limiting (OLg), etc. [4–25]. Two main properties of the nonlinear materials viz., the nonlinear index of refraction (NIR) and response times need to be determined. The SSPM and Z-scan techniques were used extensively for these purposes since 1967 [26–31]. The first technique leads to the determination of the medium total index of refraction change and its NIR [32] while the second one leads to the calculation of the nonlinear absorption coefficient (NAC), NIR and number of ONL parameters [3].

The absorption of part of incident laser beam energy with Gaussian extent by the medium leads to a bell-like heat distribution with the maximum temperature be on the axis of the laser beam direction of propagation and minimum away from the axis. Such temperature distribution leads to change in the medium index of refraction hence a phase change of the laser beam minics the transverse distribution of the laser beam occur. The absorption leads to two types of thermal currents within the nonlinear medium viz., conduction current horizontally and convection current vertically.

Schiff bases are organic compounds constituted by a condensation reaction of amine and various active carbonyl groups connected by an azomethine (–N═CH–) bond, serves as the principal moiety for a family of aromatic azomethine compounds [33]. In general, Schiff bases are of great importance in organic and pharmaceutical fields due to their wide and efficient applications in these areas [34]. Due to the important exploitations of Schiff base compounds in varied applications viz., image systems, phase conjugation, optical limiting, optical switching, and optical data storage etc. [35], these compounds have attracted intense efforts to discover their ONL properties such as their nonlinear absorptions, and NIR, etc [36,37].

On the other hand, Schiff bases that derived from amino acids and different active carbonyl groups are important for their diverse applications [38]. The amino acid Schiff bases are in chemistry use as

* Corresponding author.
E-mail address: qusayali64@yahoo.co.in (Q.M.A. Hassan).

https://doi.org/10.1016/j.optmat.2021.111750
Received 18 October 2021; Received in revised form 29 October 2021; Accepted 2 November 2021

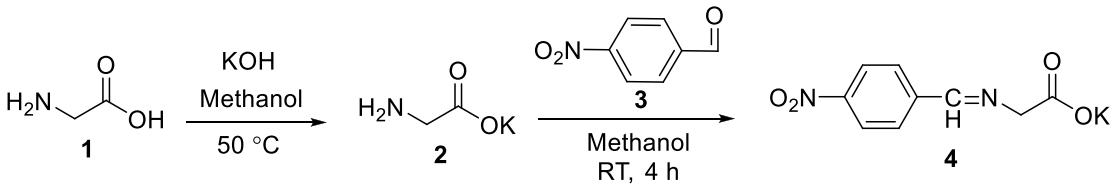

Fig. 1. Synthetic route of amino acid (glycine) Schiff base **4**.

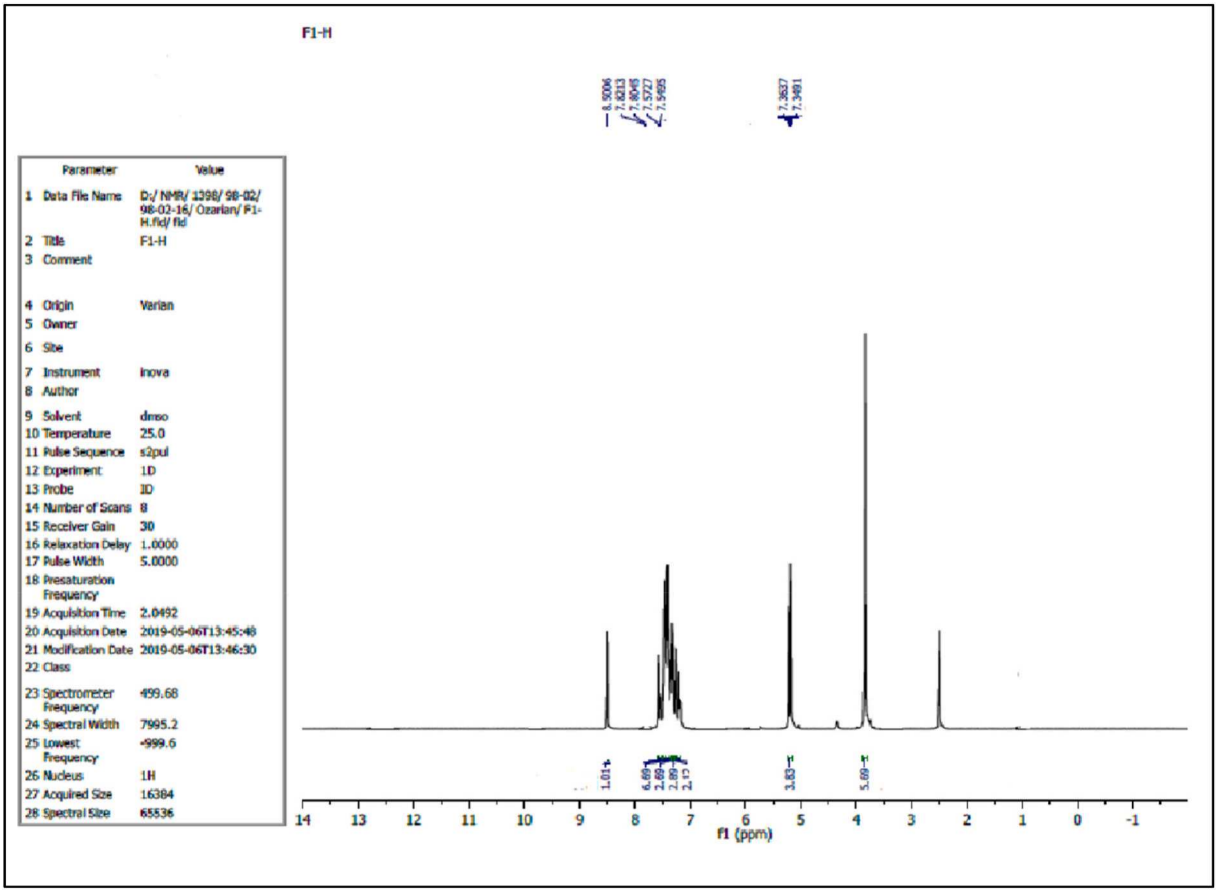

Fig. 2. Amino acid Schiff base salt **4** ^{1}H NMR spectrum.

versatile building blocks in organic synthesis with pronounced wide range of chemical applications [39,40]. Although the synthesis of amino acid Schiff bases has not been emerging to be combined with optical applications, so far some articles described various synthesis methodologies to synthesize amino acid Schiff bases [41]. Generally, the common methodology to prepare Schiff base compounds includes a simple reaction of equimolar equivalents between amines and aldehydes or ketones in ethanol, then refluxing the mixture reaction for some appropriate times. The precipitated products would be easily filtered, dried, and isolated. When an amino acid is employed as an amine component, the used methodology could not be so straightforward since the amino acid has zwitterionic properties producing in a weak nucleophilic amino moiety. Therefore, some modifications for the classic methodology have been reviewed, for instance, sodium or potassium hydroxide or anhydrous sodium sulfate was conducted to an ethanolic solution of the amino acid in order to enhance its nucleophilic property [42]. Furthermore, the synthesis of Schiff base from chiral amino acids normally offers chiral amino acid Schiff bases under basic conditions that are identified to enhance racemization of azomethine compounds [43]. Thus, we synthesize amino acid Schiff base **4** from glycine **1** as non chiral amino acid and 4-nitro benzaldeyhyde **3** (Fig. 1), and to investigate their spectroscopic, theoretical, and ONL properties.

In the present work amino acid (glycine) - 4-nitro benzaldeyhyde derived Schiff base compound was synthesized and fully characterized by magnetic nuclear resonance, infrared (IR) and mass, UV–visible spectroscopies. The structural geometry and melting point of amino acid Schiff base was optimized using density functional theory (DFT). The ONL properties of the Schiff base was studied via the ring diffraction

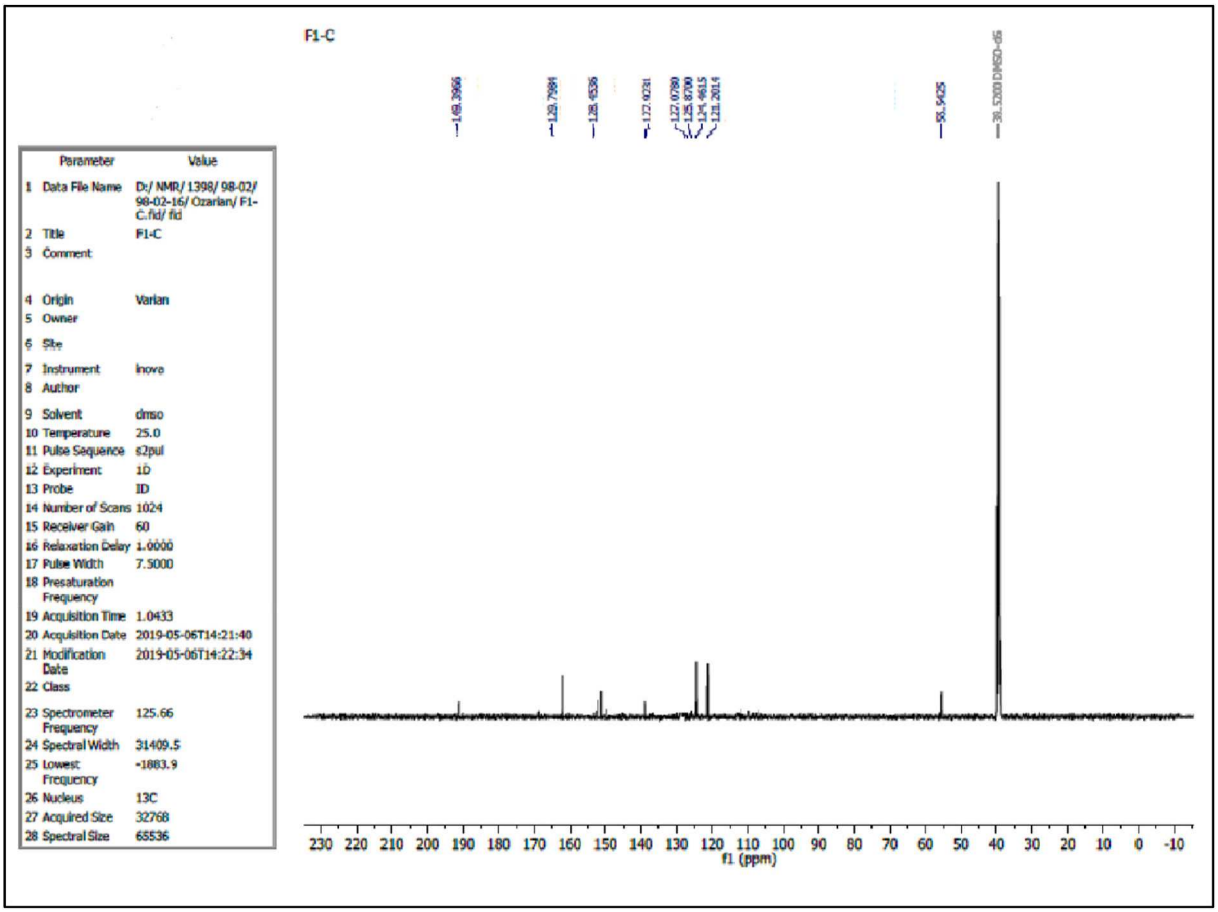

Fig. 3. Amino acid Schiff base salt **4** ^{13}C NMR spectrum.

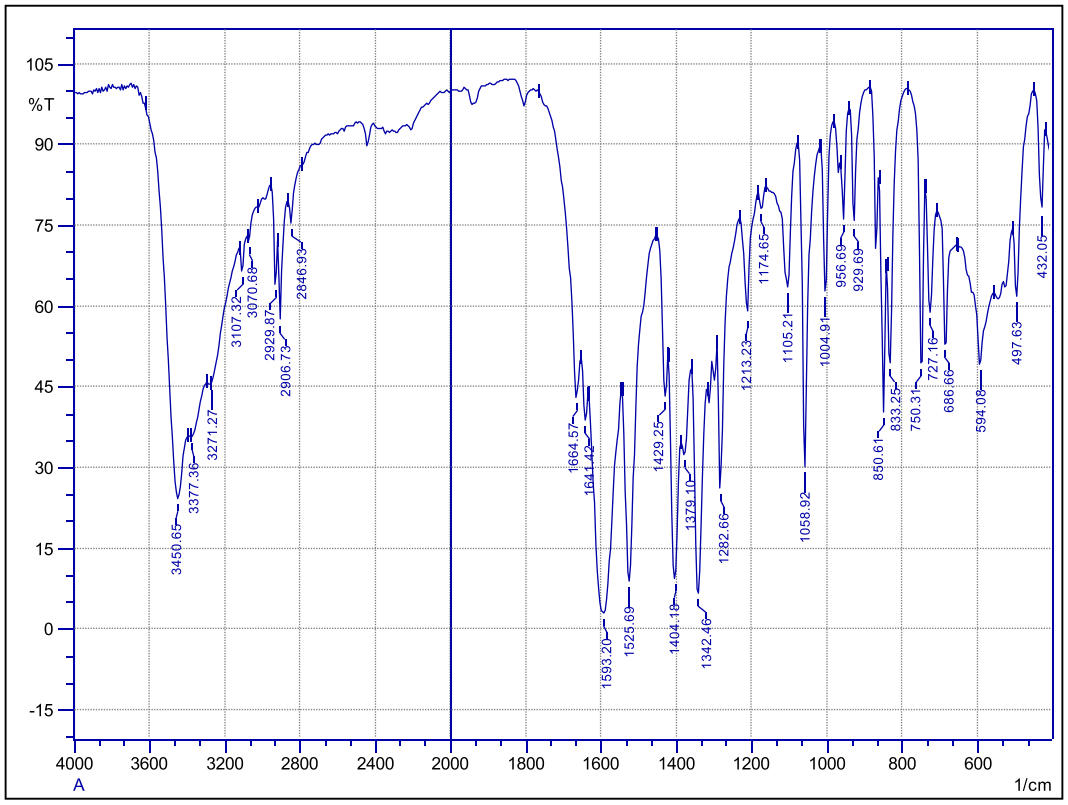

Fig. 4. Amino acid Schiff base salt **4** FT-IR spectrum.

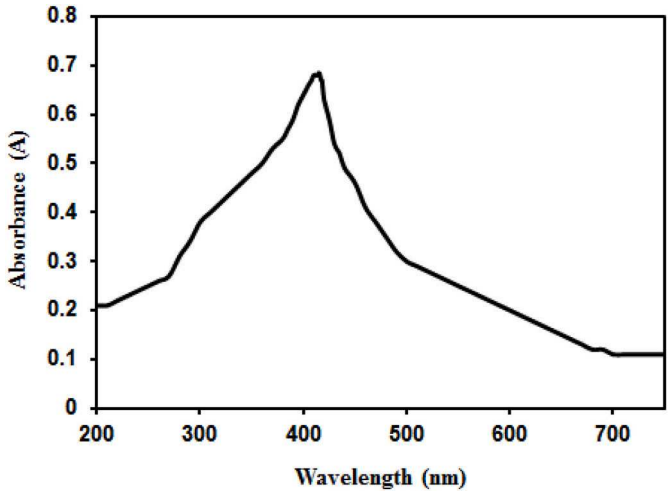

Fig. 5. Spectrum of UV–visible absorbance of the synthesized amino acid Schiff base salt **4**.

$$\alpha = 2.303\frac{A}{d} \quad (1)$$

patterns (RDPs) and Z-scan where the NIR of the Schiff base was calculated. The OLg property of the base was tested.

2. Experimental

2.1. Materials and methods

Glycine, 4-nitro benzaldeyhyde, and potassium hydroxide are commercially available chemicals as well as solvents were obtained from Sigma-Aldrich Company. Thin Layer Chromatography (TLC) (silica gel, g/uv 254) plates was employed to follow the progress of the reactions. The NMR (^{1}H and ^{13}C) spectra were obtained on spectrometer Bruker inovo AV-400 using DMSO-d_6 as standard solvent (^{1}H NMR: DMSO-d_6: δ 2.50 ppm and ^{13}C NMR: DMSO-d_6: δ 39.52 ppm). The coupling constants values (J) of protons are expressed in Hz. FT-IR spectrum was obtained using a spectrophotometer type Shimadzu FTIR-84005 infrared via KBr disc and the absorbance bands were recorded between 4000 and 600 cm^{-1}. Melting point for the synthesized amino acid Schiff base was measured using a Gallenkamp apparatus. Mass spectrum was recorded on Agilent Technologies-5975C (electrospray impact mode, 70 eV). The spectrum of UV–visible of absorbance was performed using UV-160v, Shimadzu spectrophotometer in the region between 200 and 750 nm.

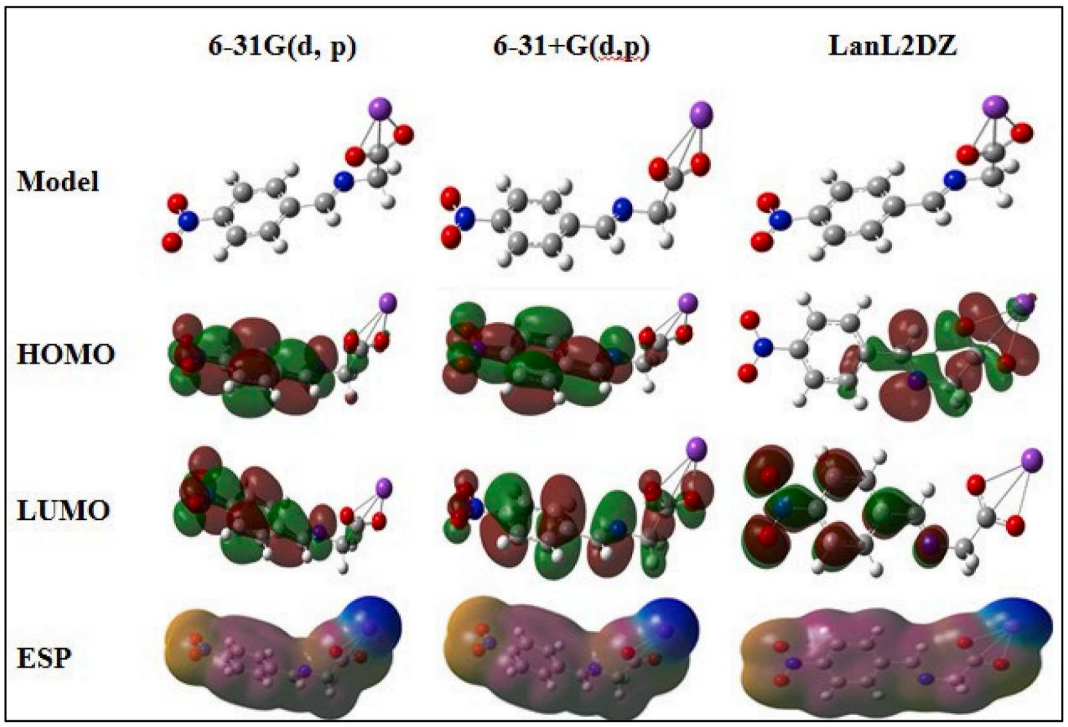

Fig. 6. Molecular model, orbital density distributions (frontier molecule), and electrostatic potentials of the synthesized amino acid Schiff base salt **4**.

Table 1
HOMO, LUMO and dipole moment values for the synthesized amino acid Schiff base salt **4** by using B3LYP with 6–31G(d,p), 6-31+G(d,p), and LanL2DZ as basis sets.

Properties	6-31G(d,p)	6-31+G(d,p)	LanL2DZ
HOMO (eV)	−5.9552	−6.3878	−5.8232
LUMO (eV)	−2.2621	−2.7320	−2.8844
Dipole moment (Debye)	11.7939	12.3851	15.6753

2.2. Synthesis of amino acid Schiff base salt (4)

At 50 °C, glycine **1** (6.7 mmol) and potassium hydroxide KOH (6.7 mmol) were dissolved in methanol (50 mL) by stirring for 30 min. Next, dissolving 4-nitro benzaldeyhyde **3** (8.5 mmol) in methanol (25 mL) and added dropwise to the content of amino acid potassium salt **2** at room temperature (RT). The mixture was stirred at RT for 4 h. Post completion the reaction as indicated by TLC, the resulting mixture solution was concentrated to 10 mL by vacuum. The precipitate of amino acid Schiff base salt emerged by adding diethyl ether (20–25 mL). The precipitate was thoroughly washed with diethyl ether for three times. Next, the resulting solid was kept in oven for 10 h at 40 °C to afford amino acid Schiff base salt **4**; yellow powder; yield 85%; m.p 172–184 °C.

2.3. NMR spectrum of the amino acid Schiff base salt 4

The ^{1}H and ^{13}C NMR spectra of the synthesized amino acid Schiff base salt **4** were measured in DMSO-d_6. The ^{1}H NMR of amino acid Schiff base salt **4** agree with the obtained structure. Proton azomethine group (–N═CH–) in amino acid Schiff base salt **4** appeared at 8.55 ppm as a singlet (s, 1H). The spectrum also shows multiplet signals at 7.15–7.54 ppm for aromatic protons (m, 4H, Ar–H), and doublet signals for CH_2

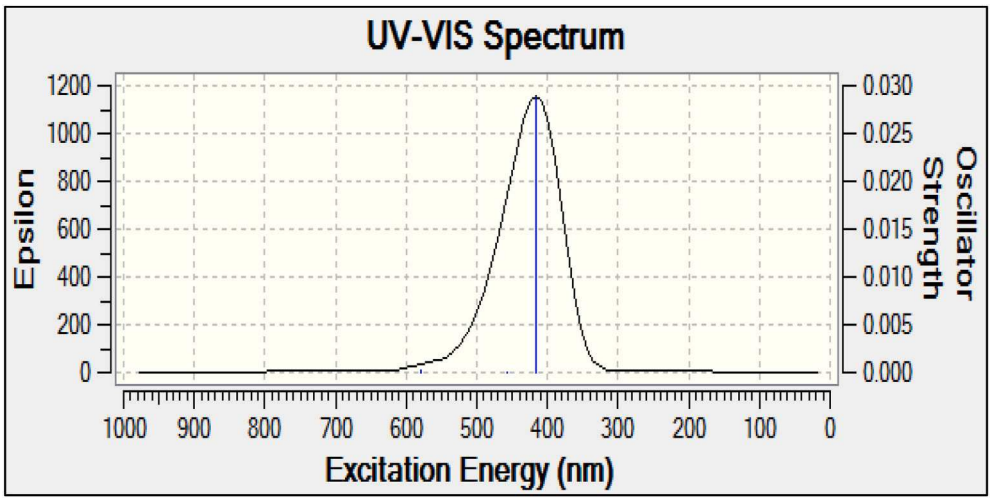

Fig. 7. The calculated UV–visible spectrum of the synthesized amino acid Schiff base salt 4 using TD-DFT with B3LYP/LanL2DZ.

Table 2
The calculated excited states of the synthesized amino acid Schiff base salt **4** using TD-DFT with B3LYP/LanL2DZ method.

Excited state HOMO → LUMO		Percentage contribution (%)	Energy(eV)	λ(nm)	f
58 → 59	1	69.962	2.1412	579.04	0.0002
57 → 59	2	70.472	2.7067	458.06	0.0000
56 → 59	3	70.489	2.9786	416.25	0.0286

group (d, $J = 2.5$ Hz, 1H, CH_2). In the ^{13}C NMR spectrum of amino acid Schiff base salt **4** the appearance of signal at the lowest field is due to carbon of the potassium carboxylate group (COOK). The other chemical shifts of ^{13}C NMR spectrum for amino acid Schiff base salt **4** appeared in the expected regions. The ^{1}H and ^{13}C NMR spectra of amino acid Schiff base salt **4** are displayed in Fig. 2 and Fig. 3.

2.4. Amino acid Schiff base salt 4 FT-IR spectrum

The important spectral bands in the FTIR spectrum of amino acid Schiff base salt **4** were performed in the solid state exploiting the KBr disc technique. Construction of amino acid Schiff base salt **4** was confirmed by its IR spectrum through the appearance of a new band of azomethine stretching band (–N═CH–) at 1641 cm^{-1}. IR spectrum of the free amino acid (glycine) shows a band at 3112 cm^{-1} that is assigned to a ν (NH_2) group and absence of this band is due to the formation of an azomethine group by condensation reaction. In addition, the bands located at regions 1593 and 1525 cm^{-1} are due to ν(C═O) and ν(C═C) of COOK group and aromatic rings respectively. Fig. 4 displays synthesized amino acid Schiff base salt **4** FTIR spectrum.

2.5. Amino acid Schiff base salt 4 mass spectrum

The synthesized amino acid Schiff base salt **4** mass spectrum shows a signal with $m/z = 245$ that is very near to its obtained molecular weight $m/z = 246$ and the other fragments show good agreement with the expected structure. Thus, the data of mass spectrum showed an identical agreement with the structure of the synthesized amino acid Schiff base salt **4.**

2.6. The UV–visible study of the amino acid Schiff base salt 4 absorbance

The synthesized amino acid Schiff base salt **4** was dissolved in DMSO at concentration of (10 mM), in all the measurements in this work. Spectrum of UV–visible of the amino acid Schiff base salt **4** solution was performed in a cell of thickness (1 mm) at RT. From the UV–visible spectrum (Fig. 5**),** it is observed that amino acid Schiff base salt **4** solution gives a maximum electronic absorption at the wavelength 415 nm that is due to π–π* electronic transition. Using the following relation [44].where d is the sample thickness, A is its absorbance and α is absorption coefficient. From Fig. 5 A = 0.38 and d = 1 mm so that α = 8.75 cm^{-1} at wavelength 473 nm of the amino acid Schiff base salt **4**.

2.7. Experimental set-ups

The set-up experimental used in this work to study the ONL properties is similar to one that can be found elsewhere [7]. In all three main experiments a cw laser beam of 473 nm obtained from a solid laser device (type SDL-473-050T) with variable output power from 0 to 66 mW, beam mode TEM00, beam divergence <1.5 mrad, power stability <5% (over 5 h), beam quality factor of 1.095, operating temperature 25 °C, and emit cw laser beam of diameter of 1.5 mm (at e^{-2}) was used as a source. A 0.1 cm thickness glass sample cell and a positive 50 mm focal

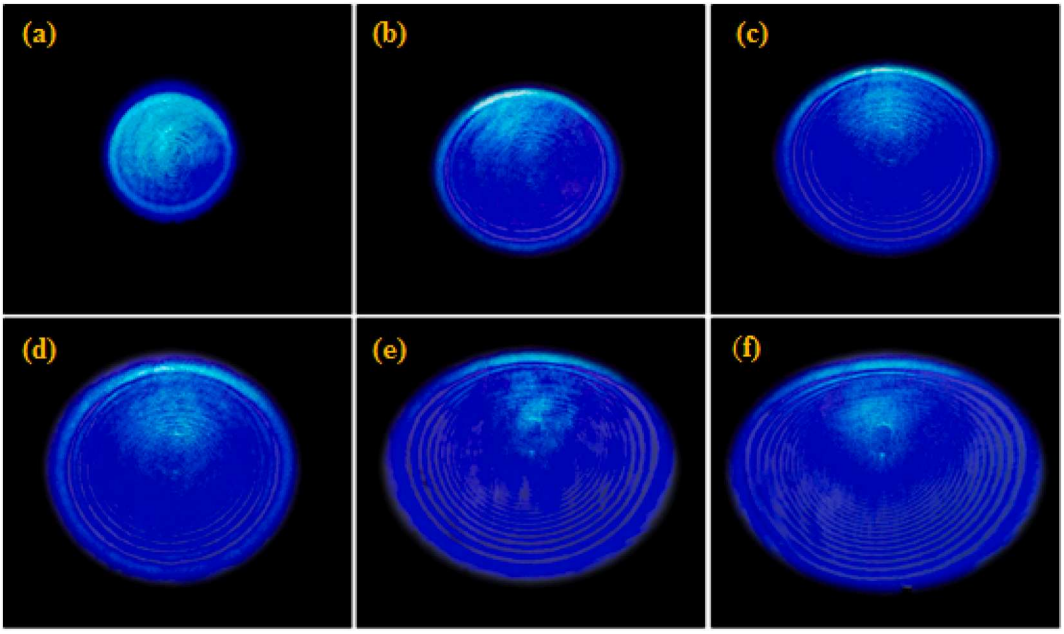

Fig. 8. Dependence of ring patterns in amino acid Schiff base salt **4** on the laser beam power input (mW):(a) 8, (b) 15, (c) 23, (d) 32, (e) 48, (f) 62.

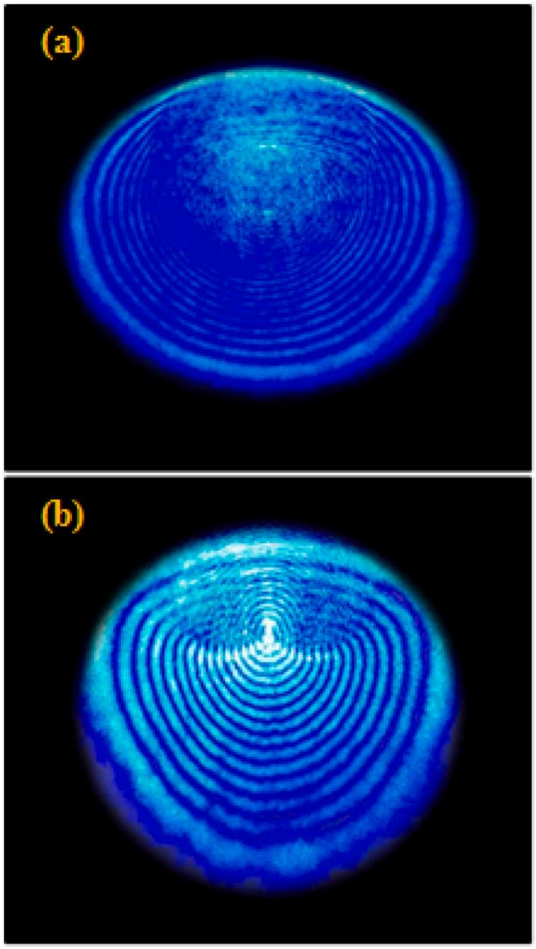

Fig. 9. Dependence of ring patterns in amino acid Schiff base salt **4** on the laser beam wave front: (a) convergent, (b) divergent, at power input 62 mW.

length glass lens was used to focus the beam onto the sample cell.

In the RDPs experiment, a semitransparent 30 × 30 cm screen used to cast the RDPs and a camera was used to capture the RDPs. In the Z-scan experiments, to sweep the sample cell from (-z) to (z), it was fixed on a translation stage passing through the lens focus (z = 0). The screen was replaced with a power meter, for the close aperture, CA, Z-scan covered with circular 2 mm diameter iris while for the open aperture, OA, Z-scan it was carried out by replacing the circular iris with a positive glass lens to capture the transmitted laser beam traversing the sample cell. In the case of OLg experiment, the sample cell was fixed at the position of valley curve of the CA-Z- scan so that the laser beam power transmitted through the sample was measured against the incident laser beam power.

3. Results

3.1. Theoretical calculations of the amino acid Schiff base salt 4

The DFT calculations include the determination of the minimum energy of geometrical structure for the synthesized amino acid Schiff base salt **4** using the Gaussian 09 program and the vibrational band was assigned by using Gauss-View (MVP) [45]. The optimization for geometrical structure of the synthesized amino acid Schiff base salt **4** was performed using the B3LYP method combined with the number of basis set level viz., 6-31G(d,p), 6-31+G(d,p), and LanL2DZ. The configured orbitals and electronic states have been acquired to investigate the highest occupied, the lowest unoccupied molecular orbitals, and electrostatic potentials surfaces (ESP) [46,47].

The frontier orbital energies (HOMO and LUMO) and molecular ESP evaluation play an important role to understand the stability of molecular structures that is very necessary to study the optical activities viz., linear and ONL properties [48,49]. The HOMO and LUMO energies reveal the reactivity of this molecule and demonstrate the eventual charge transfer that occurs in the molecule as well as the ESP were also calculated using the B3LYP method with the above basis sets, and these calculations results are shown in Fig. 6 and Table 1.

The theoretical UV–visible spectrum of the synthesized amino acid Schiff base salt **4** was carried out using TD-DFT combined with B3LYP/LanL2DZ method. The results from TD-DFT calculations showed the existence of three main electronic transitions bands at 579.04, 458.06 and 416.25 nm with (f) values of 0.0002, 0,000 and 0.0286 respectively as configured in Fig. 7. The excited states of the synthesized amino acid Schiff base salt **4** were determined by TD-DFT combined with B3LYP/LanL2DZ method are given in Table 2.

3.2. Nonlinear study

The formation of the RDPs are based on the SSPM where the interference of each two beams eminating from each two points on the Gaussian wave front of the laser beam with the phase relation $\varphi_m - \varphi_{m+1} = m\pi$, m is an integer, odd or even occurs, so that bright and dark rings appears. Fig. 8 shows the relation between the RDPs and variation of input power slowly. The patterns areas and the rings number per each pattern monotonically increases as power input increase. Each pattern appears symmetric at low input power that loses symmetry as the power input increase. Fig. 9 shows the wave front type effect of laser beam on the type of the RDP i.e. the laser beam interaction and the nonlinear medium is wave front type dependent, these results agree with work of other researchers [50]. Temporal evolution of the RDPs is shown in Fig. 10. It can be seen that at t = 0 s the spot size appears small with on rings. As time lapse the rings number and area of each pattern increases, and the RDP loses vertical symmetry due the current of convection vertically compare to the current of conduction horizontally.

The results shown in Fig. 11 are belong to the CA Z-scan. From Fig. 11, it can be seen that the curve have peak followed by a valley, i.e., the phenomena of, SDF, occurs, which point out that the sample has negative NIR. When conducting the OA Z-scan, a straight horizontal line resulted, which point out that the sample bare no NAC.

One of the purposes of preparing the amino acid Schiff base salt 4 compound was to study the possibility of using it as an optical limiter (OLr), this was achieved by conducting the OLg experiment on the amino acid Schiff base salt 4 compound using the same wavelength used in other experiments i.e. 473 nm. The compound possesses the OLr through the results obtained when conducting the OLg experiment, which is shown in Fig. 12a. As the relation between the power output and input is linear at the low input power; as the input power increased the output power become nonlinear. As the input power continued increase, the output power becomes constant. The mechanism that explains how the sample shows the behavior of the OLr is the refractive index (thermal effect), which results in the occurrence of the

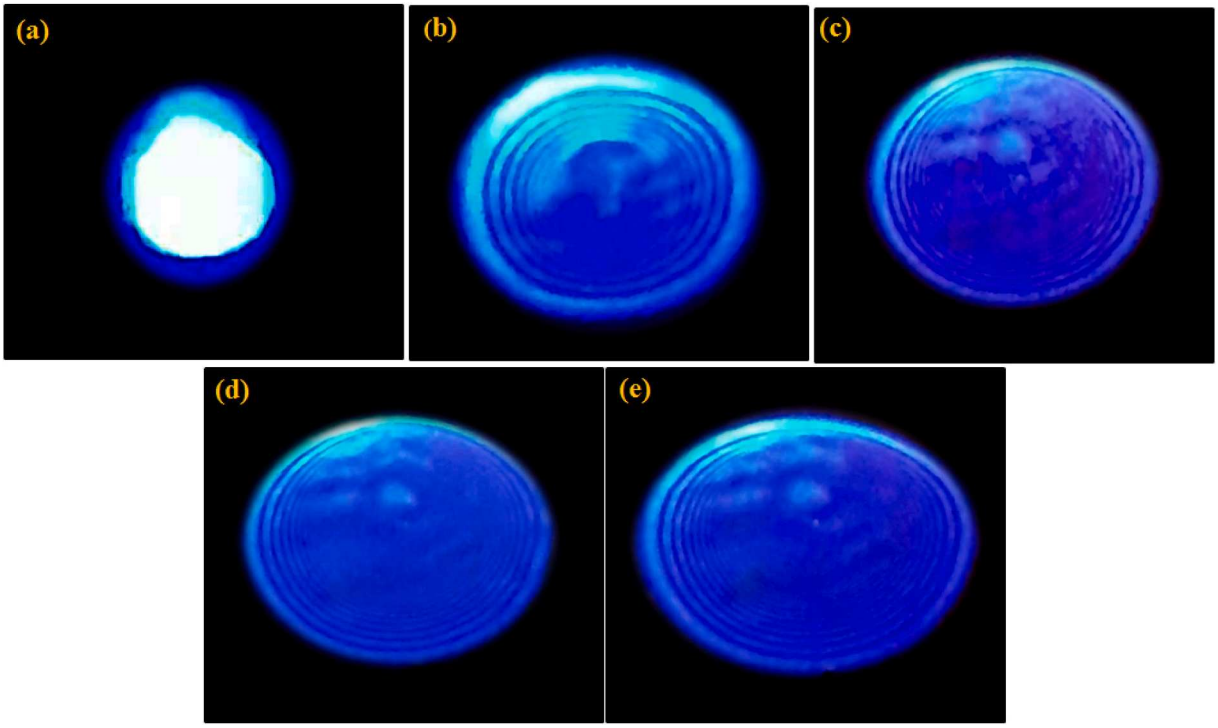

Fig. 10. Temporal evolution of a chosen RDP in amino acid Schiff base salt **4** (ms): (a) 0, (b) 250, (c) 500, (d) 750, (e) 1000 at input power 62 mW.

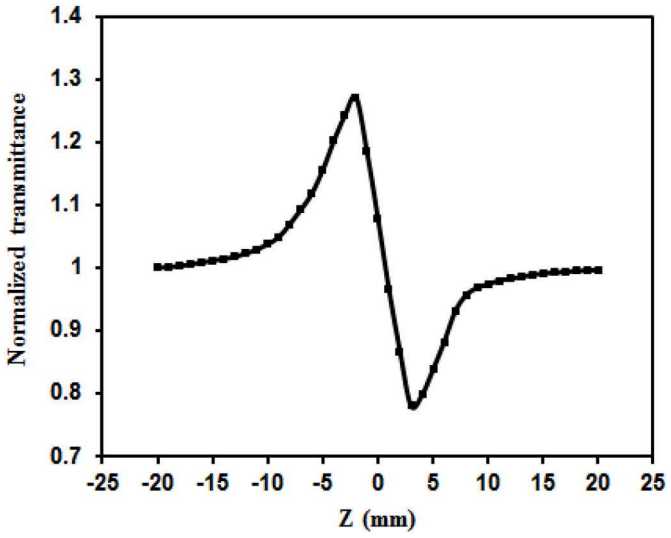

Fig. 11. Relation of the normalized laser beam power transmittance against the sample position (±z) in the CA-Zscan of amino acid Schiff base salt **4**.

$$\Delta\varphi(r) = \Delta n e^{-2r^2/\omega^2} \cdot kd$$
$$\Delta\varphi(r) = \Delta\varphi_o e^{-2r^2/\omega^2} \quad (2)$$

phenomenon of SDF of laser beam due to used cw laser beam.

3.3. Determination of the NIR of amino acid Schiff base salt 4 due to SSPM and Z-scan

As the laser beam traverses the amino acid Schiff base salt 4 it's phase suffers changes, $\Delta\varphi(r)$, which is written as follows [51]:

Δn is the total refractive index change of the medium on axis, r is the distance from the beam axis, $k = \frac{2\pi}{\lambda}$ is the beam propagation vector, λ is the wavelength of laser beam, ω is the laser beam radius, and $\Delta\varphi_o$ is phase of laser beam on the beam axis. Based on optics, the birth of one ring is an indication of the laser beam phase change by 2π radians.

For N rings the total phase change, $\Delta\varphi_o$, can be written as follows

$$\Delta\varphi_o = 2\pi N \quad (3)$$

and

$$\Delta\varphi_o = k\Delta n d \quad (4)$$

From equations (3) and (4) we have

$$\Delta n = \frac{N\lambda}{d} \quad (5)$$

And the NIR, n_2, can be written as follows

$$n_2 = \frac{\Delta n}{I} \quad (6)$$

$I = \frac{2P}{\pi\omega^2}$ is the intensity of laser beam and P is the maximum power input.

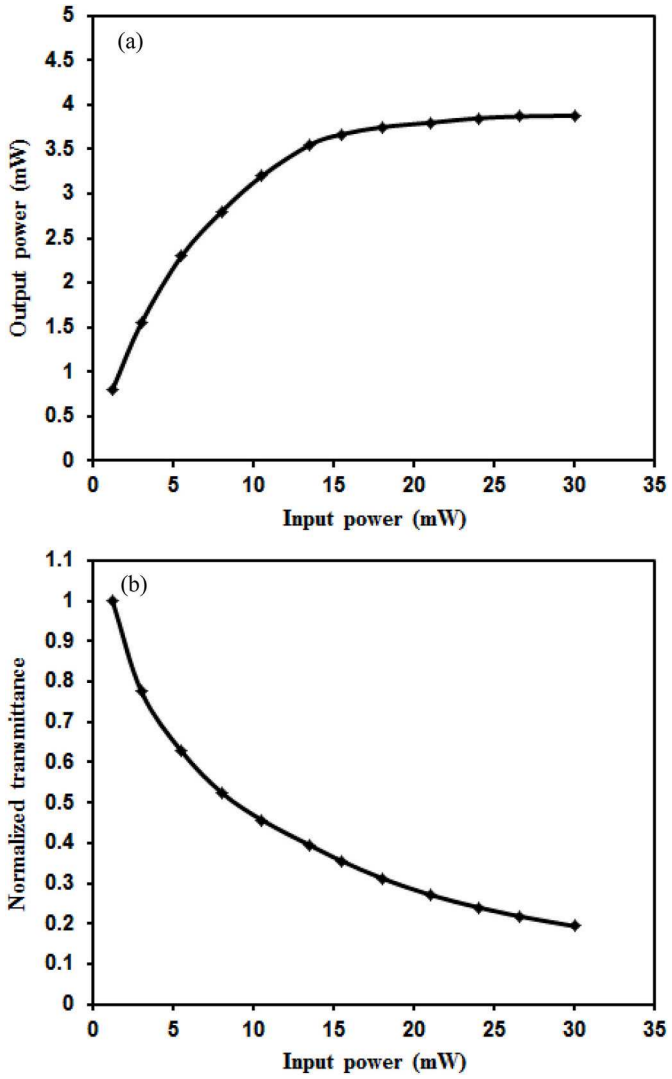

Fig. 12. (a) Relation of power transmitted of laser beam through the of amino acid Schiff base salt **4** against power input incident, (b) normalized transmittance against power input incident on the amino acid Schiff base salt **4**.

For $N = 13$, $P = 62$ mW, $\omega = 19.235$ μm, $I = 10673.6$ W/cm^2, $d = 0.1$ cm and $\lambda = 473$ nm so that $\Delta n = 6.149 \times 10^{-3}$ and $n_2 = 5.761 \times 10^{-7}$ cm^2/W.

Since in the current study a cw laser beam was used, so the nonlinearity origin of amino acid Schiff base salt **4** is thermal. The thermal nonlinearity shown by the amino acid Schiff base salt **4** can be explained as follows: When the laser beam falls on the sample, the sample will become hot as a result of absorbing part of the energy of the laser beam. As a result of this process, a thermal lens will be created, which will lead to a phase shift of the laser beam, causing the phenomenon of SDF of the laser beam. Due to the Cuppo et al. model [52] the NIR, n_2 , is given by the following relation [53].

$$n_2 = \frac{\Delta T_{p-v}\lambda}{4\pi dI} \tag{7}$$

Where ΔT_{p-v} is peak and valley transmittances difference. By finding the value of ΔT_{p-v} from Fig. 11, use of $P = 5$ mW, I = 860.7 W/cm^2 and substituting into equation (7), the value of the NIR, n_2 , of the sample is 0.21×10^{-7} cm^2/W. The variance of n_2 values due to the RDPs and the Z-scan techniques is related to the difference of input power used where it was higher in the first technique compared to the second one. Further, n_2 value depends directly on the laser beam intensity.

3.4. Determination the limiting threshold value, T_H of amino acid Schiff base salt 4

To determine whether the synthesized compound can be used as an OLr, a parameter called the limiting threshold value, T_H, was calculated which is defined as the value input power at which the transmittance is reduce to half. This value can be determined by drawing a curve of transmittance through the sample and the power input, and from this curve we find that T_H for the amino acid Schiff base salt 4 compound is 9 mW.

3.5. Simulating the RDPs in the amino acid Schiff base salt 4

When a laser light beam with Gaussian intensity extent propagate through a medium, the medium absorbs part of the laser beam energy according to its thickness, d, and linear absorption coefficient, α. The medium temperature increase, $\Delta T(x, y, t)$, leads to the refractive index variation, $\Delta n(x, y, t)$, with Gaussian distribution locally. As a result, the advanced laser beam will suffer changes in its phase, $\Delta\varphi(x, y, t)$. Let ω be the radius of the laser beam (e^{-2}), R is the beam wave front radius where the coordinate system origin was taken as the beam waist position. At the sample entrance, the electric field amplitude can be written as follows [54]:

$$U(x, y, t, z = 0) = \left(\frac{2P}{\pi\omega^2}\right)^{1/2} \exp\left(-\frac{r^2}{\omega^2}\right)\exp\left(-ik\frac{r^2}{2R}\right) \tag{8}$$

In subsection (3.2) it was noticed that asymmetries occurs to the diffraction ring patterns in the y direction. As the energy absorbed by the medium two types of thermal currents initiated, one in the horizontal direction and one in the vertical direction. When both currents are equal, the rings appeared circularly symmetric. In the vertical direction convection velocity caused by the spatial variation of the buoyancy force with the existence of gravitational force, so that the hot upper part of the rings will moved upward and replaced by a cold one that smooth the temperature gradient and decrease the change in refractive index so that the radius of the upper half of rings grew in a small ratio compared to the horizontal one. Accordingly a vertical convection velocity must be defined [54] and added to the theoretical formula used to simulate the RDPs viz., the Fresnel-Kirchhoff integral. By taking all definitions introduced into account, the complex of the electric field amplitude reads [54].

$$U(x', y', t) = \left(\frac{2P}{\pi\omega^2}\right)^{\frac{1}{2}} \frac{i\pi\omega^2}{\lambda D}\exp(ikD)\exp\left(-\frac{\alpha d}{2}\right)\int_{-\infty}^{\infty} dx \int_{-\infty}^{\infty} dy.\exp\left(-\frac{r^2}{\omega^2}\right).\exp\left[i\left(-k\frac{r^2}{2R} + \Delta\varphi(x, y, t)\right)\right].\exp\left(-ik\frac{xx' + yy'}{D}\right) \tag{9}$$

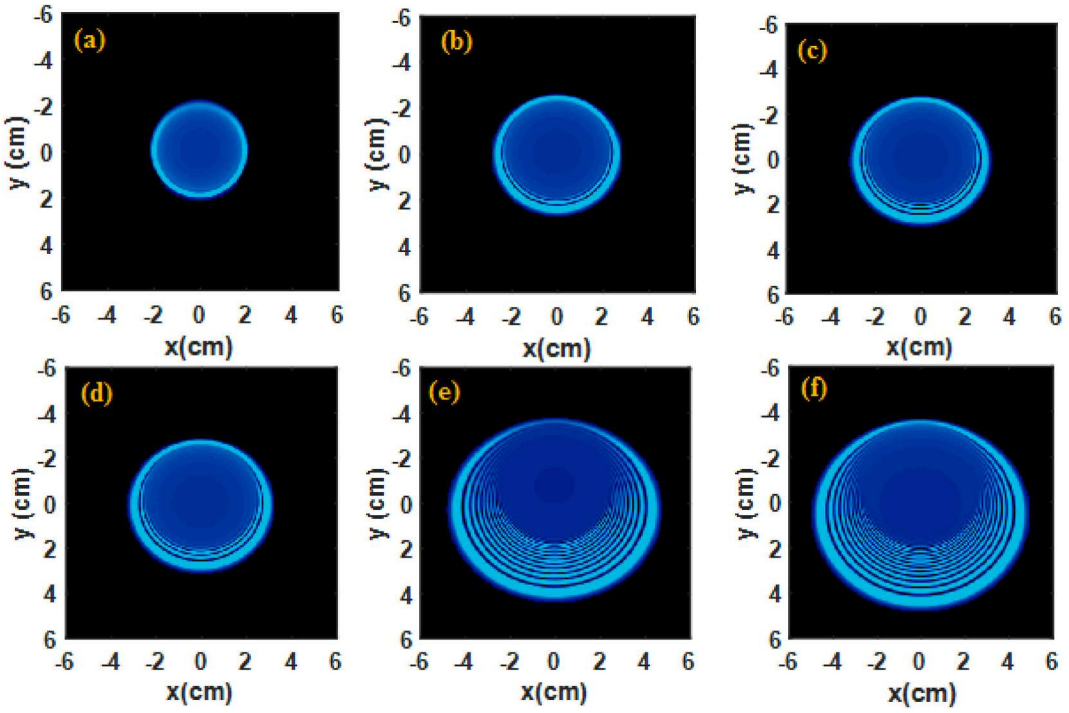

Fig. 13. Calculated dependence of RDPs of amino acid Schiff base salt 4 on inputs power (mW): (a) 8, (b) 15, (c) 23, (d) 32, (e) 48, (f) 62.

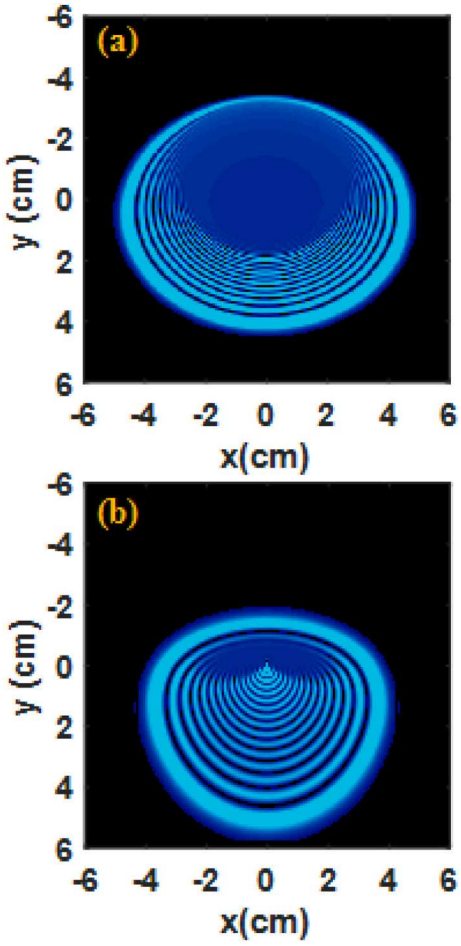

Fig. 14. Calculated dependence of the RDPs of amino acid Schiff base salt 4 on the laser beam type curvature (a)convergent (b)divergent at power input 62 mW.

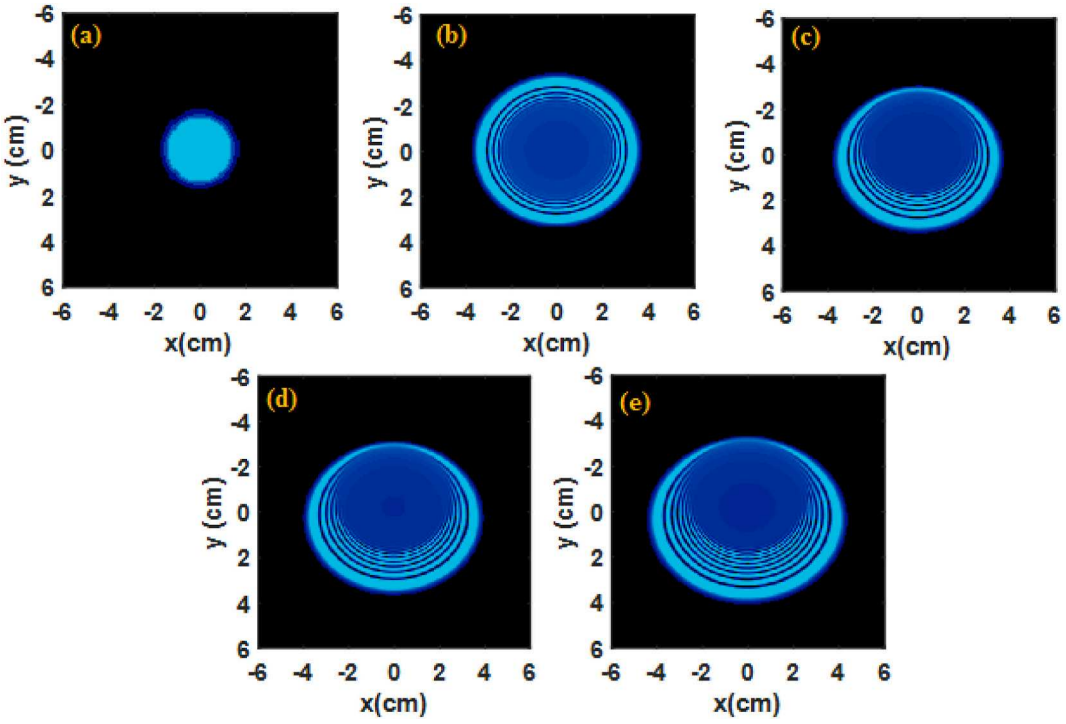

Fig. 15. Calculated temporal behavior of a chose RDPs in amino acid Schiff base salt 4, (ms) (a) 0, (b) 250, (c) 500, (d) 750, (e)1000.

$$I(x',y',t)=\left|\left(\frac{2P}{\pi\omega^2}\right)^{\frac{1}{2}}\frac{i\pi\omega^2}{\lambda D}\exp(ikD)\exp\left(-\frac{\alpha d}{2}\right)\int_{-\infty}^{\infty}dx\int_{-\infty}^{\infty}dy.\exp\left(-\frac{r^2}{\omega^2}\right).\exp\left[i\left(-k\frac{r^2}{2R}+\Delta\varphi(x,y,t)\right)\right].\exp\left(-ik\frac{xx'+yy'}{D}\right)\right|^2 \quad (10)$$

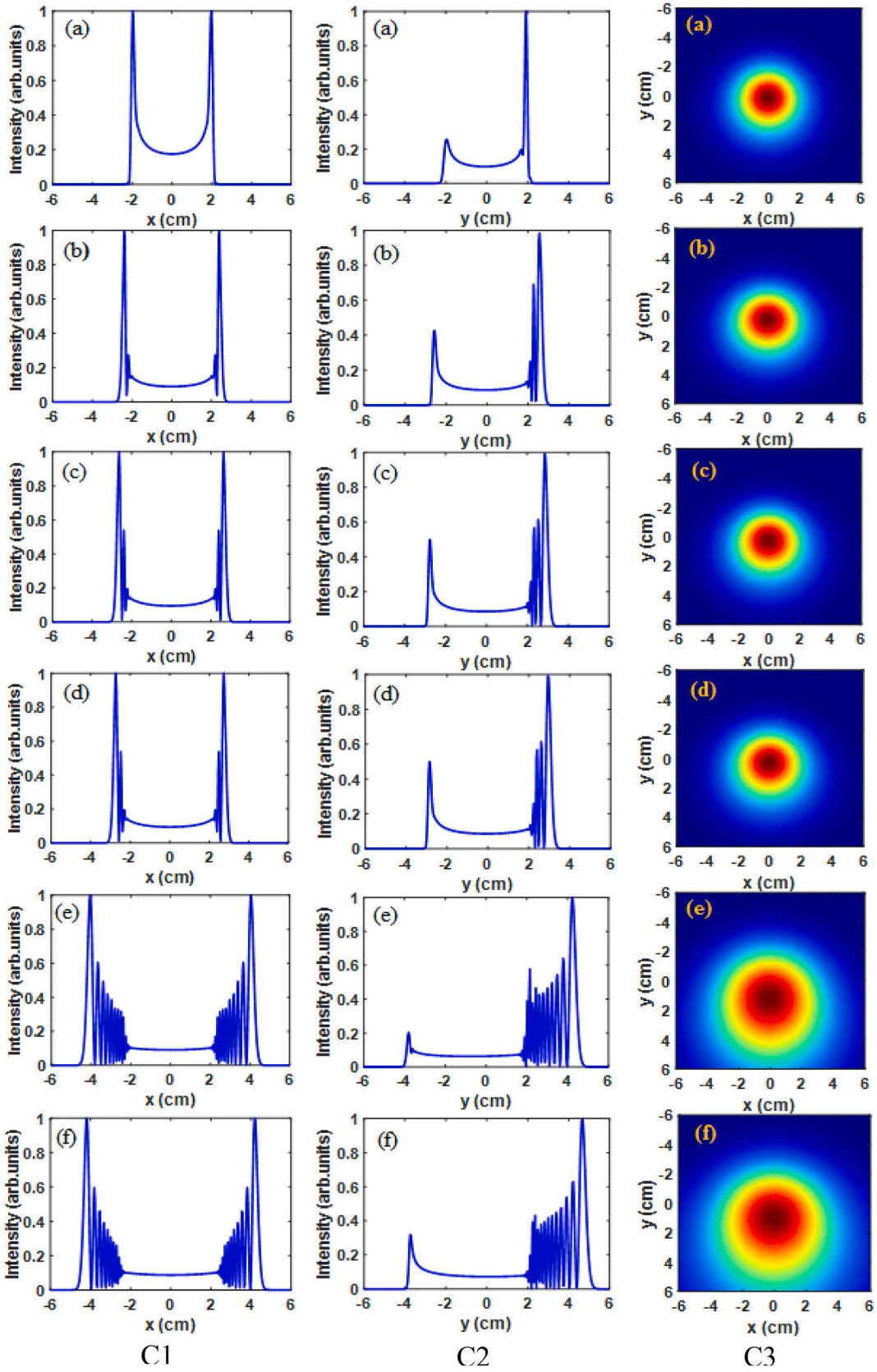

Fig. 16. Calculated intensity distribution dependence on input power C1:1d-x-axis, C2:1d-y-axis, C3:2d laser beam phase distribution, in amino acid Schiff base salt 4. (mW):(a) 8, (b) 15, (c) 23, (d) 32, (e) 48, (f) 62.

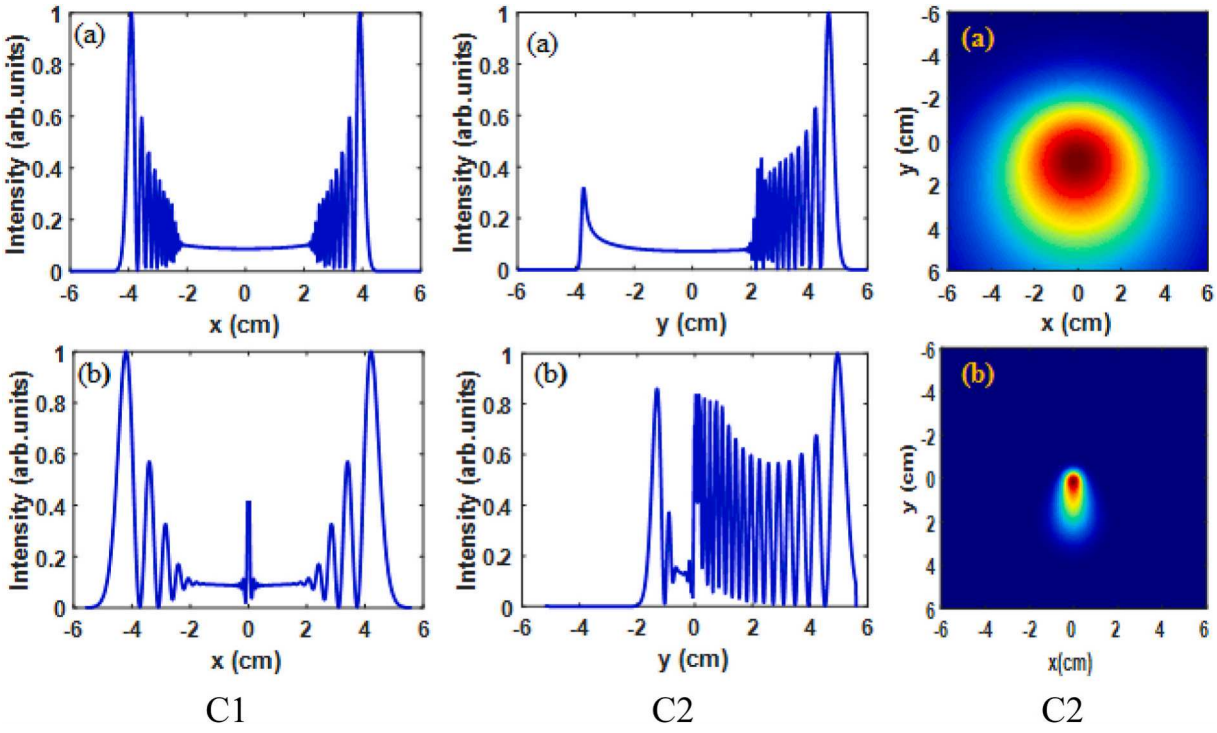

Fig. 17. Calculated dependence of intensity distribution on laser beam curvature (a) convergent and (b) divergent: C1:1d-x-axis, C2:1d-y-axis and C3:2d power input of laser beam phase at 62 mW in amino acid Schiff base salt 4.

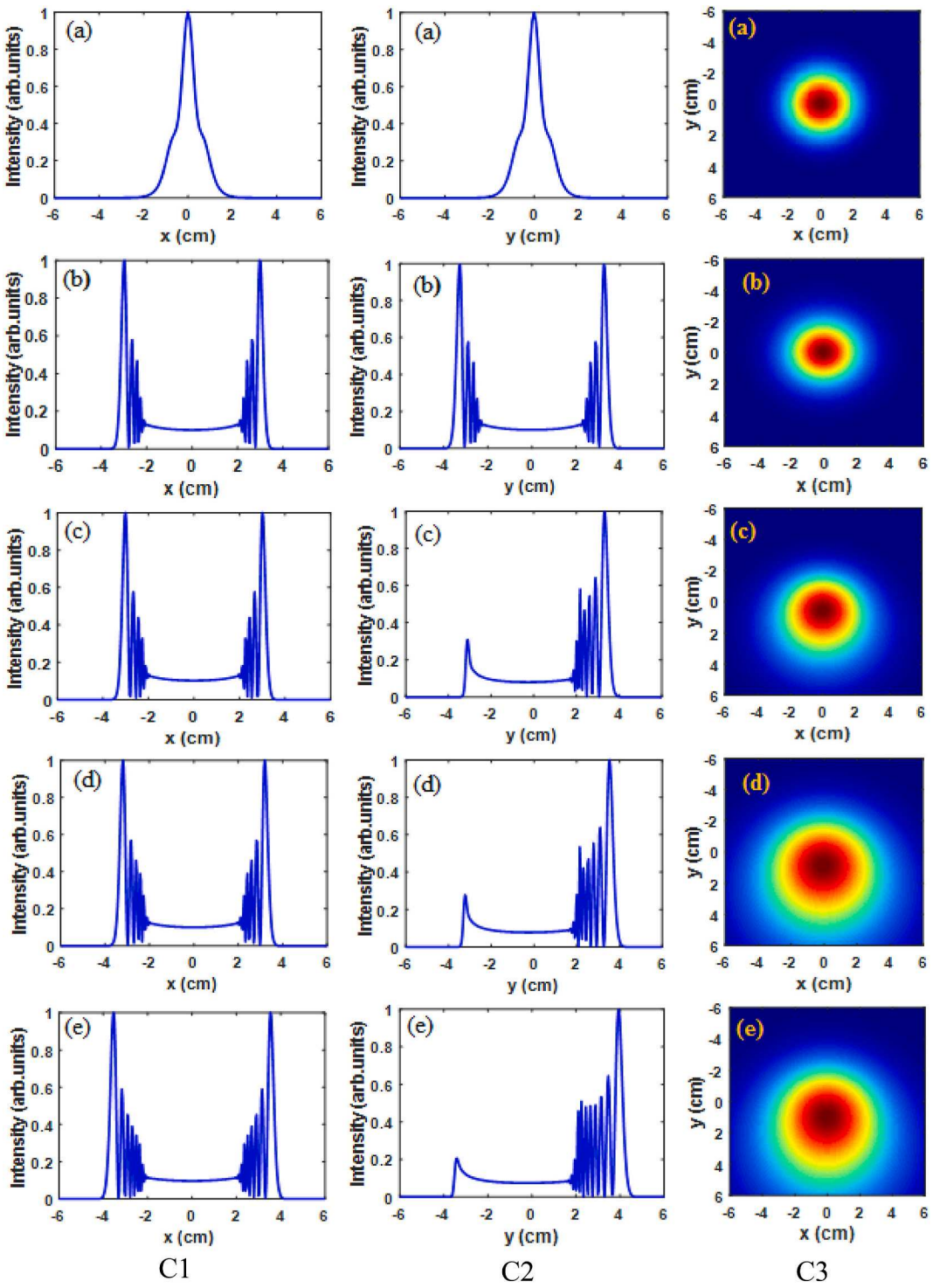

Fig. 18. Calculated temporal evolution of intensity distribution: C1:1d-x-axis, C2:1d-y-axis and C3:2d laser beam phase at power input of 62 mW in amino acid Schiff base salt 4.

Since the screen was a distance D from the exit plane of the sample cell where the spatial coordinates becomes x' and y', using the Fresnel-Kirchhoff theory, the final form of the intensity of light distributions on the screen is written as follows [54]:

Equation (10) was numerically solved using the system Mat Lab. Figs. 13–15 represents respectively the calculated dependence of the RDPs on power input, on the laser beam type curvatures and time, while Figs. 16–18 represents the calculated 1d (C1:x-axis, C2: y-axis) laser beam intensity distributions on the screen and (C3) are the laser beam phase 2d distributions for the input power used in Fig. 8, effect of the type of the laser beam wave front and temporal variation respectively. Fig. 19 shows direct comparison of experimental (blue) with theoretical (red) results for four chosen cases.

4. Conclusions

The passage of a visible cw 473 nm laser beam through synthesized

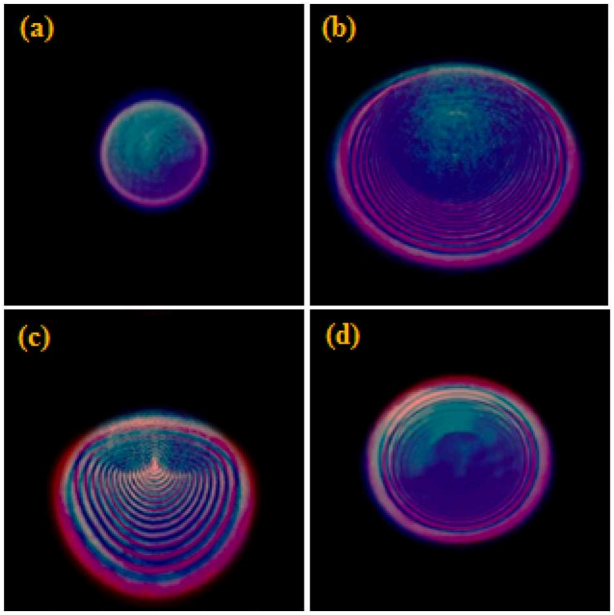

Fig. 19. Comparison of experimental (blue) and theoretical (red) results of diffraction ring pattern chose (a) ring pattern at power input 8 mW (b) RDP at power input 62 mW using divergent beam (c) RDP at power input 62 mW using convergent beam (d) RDP at time 250 ms.

amino acid(glycine) 4-nitro benzaldeyhyde-derived Schiff base have led to the generation of ring diffraction pattern, RDPs, where the nonlinear index of refraction, NIR, of the sample was determined. Based on the Z-scan the NIR was determined. The study of the optical limiting, OLg, property of the sample prove that it can be used as optical limiter, OLr. Based on the Fresnel-Kirchhoff integral numerical procedure, good theoretical results that agree with experimental one were obtained.

Declaration of competing interest

The authors declare that they have no known competing financial interests or personal relationships that could have appeared to influence the work reported in this paper.

References

[1] A.B. Villafranca, K. Saravanamuttu, Diversity and slow dynamics of diffraction ring patterns:a comprehensive study of spatial self-phase modulation in a photopolymer, J. Opt. Soc. Am. B 29 (2012) 2357–2372.
[2] M.A. Proskurnin, D.S. Volkov, T.A. Gorkova, S.W. Bendryshera, A.P. Smirnora, D. A. Nedosekin, Advances in thermal lens spectrometry, J. Anal. Chem. 70 (2015) 249–276.
[3] M. Sheik-Bahae, A.A. Said, T. Wei, D.J. Hagan, E.W. Van Stryland, Sensitive measurement of optical nonlinearities using a single beam, IEEE J. Quant. Electron. 26 (1990) 760–769.
[4] Bahjat A. Saeed, Qusay M.A. Hassan, C.A. Emshary, H.A. Sultan, Rita S. Elias, The nonlinear optical properties of two dihydropyridones derived from curcumin, Spectrochim. Acta Mol. Biomol. Spectrosc. 240 (2020) 118622, 14.
[5] Rita S. Elias, Qusay M.A. Hassan, C.A. Emshary, H.A. Sultan, Bahjat A. Saeed, Formation and temporal evolution of diffraction ring patterns in a newly prepared dihydropyridone, Spectrochim. Acta Mol. Biomol. Spectrosc. 223 (2019) 117297, 16.
[6] C.A. Emshary, Isra M. Ali, Qusay M.A. Hassan, H.A. Sultan, Linear and nonlinear optical properties of potassium dichromate in solution and solid polymer film, Physica B 613 (2021) 413014, 12.
[7] Ayat J. Kadhum, Nazar A. Hussein, Qusay M.A. Hassan, H.A. Sultan, Ahmed S. Al-Asadi, C.A. Emshary, Investigating the nonlinear behavior of cobalt (II) phthalocyanine using visible CW laser beam, Optik 157 (2018) 540–550.
[8] Qusay M.A. Hassan, Study of nonlinear optical properties and optical limiting of acid green 5 in solution and solid film, Opt Laser. Technol. 106 (2018) 366–371.
[9] S.A. Ali, Qusay M.A. Hassan, C.A. Emshary, H.A. Sultan, Characterizing optical and morphological properties of Eriochrome Black T doped polyvinyl alcohol film, Phys. Scripta 95 (11pp) (2020), 095814.
[10] C.A. Emshary, Qusay M.A. Hassan, H. Bakr, H.A. Sultan, Determination of the optical constants, nonlinear optical parameters and threshold limiting of methyl red-epoxy resin film, Physica B 622 (8) (2021) 413354.
[11] Qusay M.A. Hassan, P.K. Palanisamy, Z-scan determination of the third-order optical nonlinearity of organic dye nile blue chloride Mod, Phys. Lett. B 20 (2006) 623–632.
[12] M.F. Al-Mudhaffer, A.Y. Al-Ahmad, Qusay M.A. Hassan, C.A. Emshary, Optical characterization and all-optical switching of benzenesulfonamide azo dye, Optik 127 (2016) 1160–1166.
[13] V.S. Dneprovskii, A.I. Furtichev, V.I. Klimov, Li Shen, E.V. Nazvanova, D. K. Okorokov, U.V. Vandishev, Nonlinear optical properties of CdS and optical bistability, Phys. Status Solidi 150 (1988) 839.
[14] R. Sharma, G.P. Singh, Optical solitons and applications thereof, Int. J. Electron. Commun. Instrum. Eng. Res. Dev. 4 (2014) 71–76.
[15] Qusay M.A. Hassan, R.K.H. Manshad, Surface morphology and optical limiting properties of azure B doped PMMA film, Opt. Mater. 92 (2019) 22–29.
[16] Amjad F. Abdulkader, Qusay M.A. Hassan, Ahmed S. Al-Asadi, H. Bakr, H. A. Sultan, C.A. Emshary, Linear, nonlinear and optical limiting properties of carbon black in epoxy resin, Optik 160 (2018) 100–108.
[17] Qusay M.A. Hassan, Two-photon absorption-based optical limiting in 2-(2-methoxybenzyllideneamino)-5-methylphenylmercuric chloride-doped PMMA film, Mod. Phys. Lett. B 28 (10) (2014) 1450079.
[18] R.K.H. Manshad, Qusay M.A. Hassan, Optical limiting properties of magenta doped PMMA under CW laser illumination, Adv. Appl. Sci. Res. 3 (2012) 3696–3702.
[19] Qusay M.A. Hassan, R.K.H. Manshad, Optical limiting properties of Sudan red B in solution and solid film, Opt. Quant. Electron. 47 (2015) 297–311.
[20] Qusay M.A. Hassan, Nonlinear optical and optical limiting properties of chicago sky blue 6B doped PVA film at 633nm and 532 nm studied using a continuous wave laser, Mod. Phys. Lett. B 22 (2008) 1589–1597.
[21] S. Manickasundaram, P. Kannan, R. Kumaran, R. Velu, P. Ramamurthy, Qusay M. A. Hassan, P.K. Palanisamy, S. Senthil, S. Sriman Narayanan, Holographic grating studies in pendant xanthene dyes containing poly(alkyloxymethacrylate)s, J. Mater. Sci. Mater. Electron. 22 (2011) 25–34.
[22] S. Manickasundaram, P. Kannan, Qusay M.A. Hassan, P.K. Palanisamy, Azo dye based poly(alkyloxymethacrylate)s and their spacer effect on optical data storage, J. Mater. Sci. Mater. Electron. 19 (2008) 1045–1053.
[23] S. Manickasundaram, P. Kannan, Qusay M.A. Hassan, P.K. Palanisamy, Holographic grating formation in poly(methacrylate) containing pendant xanthene dyes, Optoelec. Adv. Mat. Rap. Commun. 2 (2008) 324–331.
[24] Qusay M.A. Hassan, P.K. Palanisamy, S. Manickasundaram, P. Kannan, Sudan IV dye based poly(alkyloxymethacrylate)films for optical data storage, Opt Commun. 267 (2006) 236–243.
[25] Qusay M.A. Hassan, P.K. Palanisamy, Optical phase conjugation by degenerate four-wave mixing in basic green 1 dye-doped gelatin film using He–Ne laser, Opt Laser. Technol. 39 (2007) 1262–1268.
[26] W.R. Callen, B.G. Huth, R.H. Pantell, Optical patterns of thermally self-defocused light, Appl. Phys. Lett. 11 (1967) 103–105.
[27] Ghufran M. Shabeeb, C.A. Emshary, Qusay M.A. Hassan, H.A. Sultan, Investigating the nonlinear optical properties of poly eosin-Y phthalate solution under irradiation with low power visible CW laser light, Physica B 578 (13pp) (2020) 411847.
[28] Mahmoud Sh Hussain, Qusay M.A. Hassan, H.A. Sultan, Ahmed S. Al-Asadi, T. Hani, C.A. Chayed, Emshary, Preparation, characterization, and study of the nonlinear optical properties of a new prepared nanoparticles copolymer, Mod. Phys. Lett. B 33 (2019) 1950456 (17 pp).
[29] Faeza A. Almashal, Mohammed Q. Mohammed, Qusay M.A. Hassan, C.A. Emshary, H.A. Sultan, Adil M. Dhumad, Spectroscopic and thermal nonlinearity study of a Schiff base compound, Opt. Mater. 100 (12pp) (2020) 109703.
[30] Kh A. Al-Timimy, Qusay M.A. Hassan, H.A. Sultan, C.A. Emshary, Solvents effect on the optical nonlinear properties of the Sudan iv, Optik 224 (15) (2020) 165398.
[31] Dakhil Zughayir Mutlaq, Qusay M.A. Hassan, H.A. Sultan, C.A. Emshary, The optical nonlinear properties of a new synthesized azo-nitrone compound, Opt. Mater. 113 (2021) 110815, 13 pp).
[32] Qusay M.A. Hassan, C.A. Emshary, H.A. Sultan, Investigating the optical nonlinear properties and limiting optical of eosin methylene blue solution using a cw laser beam, Phys. Scripta 96 (2021), 095503(15 pp).
[33] Faeza Abdulkreem Almashal, Zainab Taha Al-Abdullah, Ahmed Majeed Jassem, Schiff base synthesis as a capping agent for green synthesized silver nanoparticles, Egypt. J. Chem. 63 (2020) 813–821.
[34] AhmedM. Jassim, Synthesis and characterization of novel Schiff bases and evaluation of corrosion inhibitors and biological activity, Univ. Thi-Qar. J. Science. 3 (2012) 64–75.
[35] Vahideh Hadigheh-Rezvan, Bahareh Pilevar-Maleki, Structural and optical properties of some 5, 8-diaminoquinoxaline Schiff bases: quantum chemical calculations, Chem. Sin. 9 (2018) 544–554.
[36] Ahmed Majeed Jassem, Qusay M.A. Hassan, C.A. Emshary, H.A. Sultan, Faeza abdulkareem almashal, wisam abdulhassan radhi, synthesis and optical nonlinear properties performance of azonaphthol dye, Phys. Scripta 96 (2020), 025503 (20 pp).
[37] B. Derkowska-Zielinska, M. Barwiolek, C. Cassagne, G. Boudebs, Nonlinear optical study of Schiff bases using Z-scan technique, Opt Laser. Technol. 124 (2020) 7, 105968.
[38] Li Yang, Jianfang Dong, Peiran Zhao, Ping Hu, Dawei Yang, Lei Gao, Lianzhi Li, Synthesis of amino acid Schiff base nickel (II) complexes as potential anticancer drugs in vitro, Bioinorgan. Chem. Appl. 2020 (2020). ID 8834859(15 pp).

[39] Martin J. O'Donnell, Benzophenone Schiff bases of glycine derivatives: versatile starting materials for the synthesis of amino acids and their derivatives, Tetrahedron 75 (2019) 3667–3696.
[40] Daria S. Timofeeva, Armin R. Ofial, Herbert Mayr, Nucleophilic reactivities of Schiff base derivatives of amino acids, Tetrahedron 75 (2019) 459–463.
[41] H. Saleem, Y. Erdogdu, S. Subashchandrabose, V. Thanikachalam, J. Jayabharathi, N. Ramesh Babu, Structural and vibrational studies on (E)-2-(2-hydroxy benzyliden amino)-3-phenyl propionic acid using experimental and DFT methods, J. Mol. Struct. 1030 (2012) 157–167.
[42] Claudia Fattuoni, Sarah Vascellari, Tiziana Pivetta, Synthesis, protonation constants and biological activity determination of amino acid–salicylaldehyde-derived Schiff bases, Amino Acids 52 (2020) 397–407.
[43] Martin J. O'Donnell, Robin L. Polt, A mild and efficient route to Schiff base derivatives of amino acids, J. Org. Chem. 47 (1982) 2663–2666.
[44] Uhood J. Al-Hamdani, Qusay M.A. Hassan, C.A. Emshary, H.A. Sultan, Adil Muala Dhumad, A. Afrah, Al-Jaber, All optical switching and the optical nonlinear properties of 4-(benzothiazolylldiazenyl)-3-chlorophenyl 4-(nonylthio)benzoate (EB-3Cl), Optik 248 (2021) 168196, 17.
[45] Renata Świsłocka, Ewa Regulska, Joanna Karpińska, Grzegorz Świderski, Włodzimierz Lewandowski, Molecular structure and antioxidant properties of alkali metal salts of rosmarinic acid, Experimental and DFT studies, Molecules 24 (2019) 2645.
[46] Adil Muala Dhumad, Qusay M.A. Hassan, C.A. Emshary, Tarek Fahad, Nabeel A. Raheem, H.A. Sultan, Nonlinear optical properties investigation of a newly synthesised Azo-(β)- diketone dye, J. Photochem. Photobiol. Chem. 418 (2021) 113429, 17.
[47] A.M. Jassem, A.H. Raheemah, W.A. Radhi, A.M. Alid, H.A. Jaber, Highly diastereoselective metal-free catalytic synthesis of drug-like spiroimidazolidinone, Russ. J. Org. Chem. 55 (2019) 1598–1603.
[48] Adil Muala Dhumad, Qusay M.A. Hassan, Tarek Fahad, C.A. Emshary, Nabeel A. Raheem, H.A. Sultan, Synthesis, structural characterization and optical nonlinear properties of two azo-β-diketones, J. Mol. Struct. 1235 (2021) 130196 (9 pp).
[49] H.A. Sultan, Adil Muala Dhumad, Qusay M.A. Hassan, Tarek Fahad, C.A. Emshary, Nabeel A. Raheem, Synthesis, characterization and the nonlinear optical properties of newly synthesized 4-((1, 3-dioxo-1-phenylbutan-2-yl) diazenyl) benzenesulfonamide, Spectrochim. Acta Mol. Biomol. Spectrosc. 251 (2021) 119487 (15 pp).
[50] E. Santamato, Y.R. Shen, Field curvature effect on the diffraction ring pattern of a laser beam dressed by spatial self-phase modulation in a nematic film, Opt. Lett. 9 (1984) 564–566.
[51] K. Ogusu, Y. Kohtani, H. Shao, Laser-induced diffraction rings from an absorbing solution, Opt. Rev. 3 (1996) 232–234.
[52] F.L.S. Cuppo, A.M.F. Neto, S.L. Gómez, P. Palffy-Muhoray, Thermal-lens model compared with the Sheik-Bahae formalism in interpreting Z-scan experiments on lyotropic liquid crystals, J. Opt. Soc. Am. B 19 (2002) 1342–1348.
[53] K. Sendhil, C. Vijayan, M.P. Kothiyal, Low-threshold optical power limiting of cw laser illumination based on nonlinear refraction in zinc tetraphenyl porphyrin, Opt Laser. Technol. 38 (2006) 512–515.
[54] R. Karimzadeh, Spatial self-phase modulation of a laser beam propagation through liquids with self-induced natural convection flow, J. Opt. 14 (2012), 095701(9 pp).